

Experimental and theoretical study of absorption of femtosecond laser pulses in interaction with solid copper targets

S. E. Kirkwood,¹ Y. Y. Tsui,¹ R. Fedosejevs,¹ A. V. Brantov,² and V. Yu. Bychenkov²

¹*Department of Electrical and Computer Engineering, University of Alberta, Edmonton, Alberta, Canada T6G 2V4*

²*P. N. Lebedev Physics Institute, Russian Academy of Science, Leninskii Prospect 53, Moscow 119991, Russia*

(Received 14 November 2008; revised manuscript received 4 February 2009; published 27 April 2009)

The reflectivity of near-infrared 150 fs laser pulses from copper targets has been measured in the intensity range of $6 \times 10^{11} - 1.6 \times 10^{14} \text{ W cm}^{-2}$, showing a drop in reflectivity versus intensity as the target is heated. A simple semianalytical model of femtosecond electron heating and resultant optical absorption is developed to describe the time dependent and integral reflectivity covering the range from cold metal response to hot plasma response. The model is in good agreement with experimental ultrafast reflectivity measurements over the intensity range studied.

DOI: [10.1103/PhysRevB.79.144120](https://doi.org/10.1103/PhysRevB.79.144120)

PACS number(s): 52.38.Dx, 72.15.Eb, 78.40.Kc, 78.68.+m

I. INTRODUCTION

Research into the femtosecond interaction of pulses with bulk and thin-film metals has demonstrated that the laser pulse leads to transient heating of the electron subsystem out of thermal equilibrium with the lattice subsystem.¹⁻³ The electron subsystem subsequently equilibrates with the lattice subsystem on the time scale of several picoseconds, eventually leading to ablation of material at higher intensities. Thus, the process of light absorption and target ablation have different time scales, and can be considered independent of each other with energy transfer among the subsystems divided into several stages. Initially, the target electrons absorb the laser energy in a thin skin layer while the lattice remains cold. The electrons then conduct heat inward, removing energy from the skin layer. At the same time the electrons transfer their energy to the lattice throughout the electron heat penetration depth until both subsystems reach local thermal equilibrium. In the case of femtosecond laser-pulse interactions, the absorption of laser radiation occurs on a time scale of the pulse duration before any significant hydrodynamic motion (ablation) can occur. Such hydrodynamic response of the target surface has characteristically been observed on the time scale of tens of picoseconds.⁴

In this paper, a model of ultrafast laser absorption in a noble metal is proposed, which accounts for the strongly nonequilibrium state of the irradiated metal during the laser pulse as it undergoes a fast transition from a solid metal to a plasma at moderate irradiation intensities of $10^{11} - 10^{14} \text{ W cm}^{-2}$. To date, it has been assumed that absorption remains constant for femtosecond pulses in this intensity range because the pulse energy is deposited before any plasma or material dynamics can take place.^{1,3,5,6} We do not study the subsequent stage of thermal equilibration between the electron and lattice subsystems, and plasma expansion that predominantly occurs after the femtosecond pulse has finished. This coupling and expansion phase is not necessary for the description of femtosecond laser-pulse absorption dynamics. The results of the model are compared to experimental measurements of reflectivity of 150 fs 800 nm pulses from smooth copper film targets.

Understanding the dynamics of absorption is very important in many current application areas of femtosecond pulses

at moderate intensities including micromachining and laser induced breakdown spectroscopy.⁷⁻¹⁰ Despite its overall importance, there are few studies where absorption dynamics of femtosecond pulses have been studied in the moderate ($10^{12} - 10^{15} \text{ W cm}^{-2}$) intensity range of interest for these applications. Studies have been reported as a function of intensity for aluminum, copper, and gold at 400 nm for 150 fs pulses at intensities of $10^{13} - 10^{17} \text{ W cm}^{-2}$ by Price *et al.*,¹¹ and as a function of angle of incidence by Fedosejevs *et al.*¹² at 248 nm for 250 fs pulses. As reported here we measure the absorption as a function of incident intensity for 800 nm 150 fs [full width at half maximum (FWHM)] pulses incident on fresh copper thin-film surfaces in the range of intensities from $6 \times 10^{11} - 2 \times 10^{14} \text{ W cm}^{-2}$, which is at the wavelength and intensity range of interest for many femtosecond micromachining and related applications. Absorption and heating in this intensity range is also of interest in the creation of preplasma conditions for many ultrahigh intensity ($10^{18} - 10^{20} \text{ W cm}^{-2}$) laser experiments where the leakage contrast ratio is on the order of $10^{-6} - 10^{-8}$.

When weak to moderate intensity laser pulses reach a metal target, they are absorbed in a surface layer under conditions of collisional absorption which are typical for the laser-metal and laser-plasma interactions at the electron temperatures in the eV range, $T_e \lesssim 100 \text{ eV}$. The absorption coefficient is defined by the effective collision frequency which is a function of T_e . During laser-matter interaction at laser intensities $< 10^{15} \text{ W cm}^{-2}$, the electron temperature changes from room temperature up to a few hundreds of eV. In this temperature range the effect of spatial dispersion is small whereas, for short laser pulses of relativistic intensities, it is important because the electron temperature can be as high as several keV. The latter is not a subject of our study.

To describe laser absorption one has to know the collision frequency over a broad temperature range. The model often used is based on interpolation between two well-known limiting cases, corresponding to the Coulomb electron-ion collisions for the hot plasma and the electron-phonon collisions for the cold solid.¹³ For the cold solid, the classical electron-phonon collision frequency is defined by the lattice temperature, making it independent of the electron temperature and effectively constant during a laser pulse due to the relatively

low electron-lattice energy exchange rate. Therefore electron-phonon collision frequency cannot explain the increase in absorption with temperature which is typical for most experiments, e.g., Refs. 11 and 14. In the case of short pulse laser-matter interaction, where the electron temperature is much higher than the lattice temperature, it is also important to account for the effect of electron-electron collisions^{15–19} which will increase the absorption. The frequency of electron-electron collisions is comparable to the electron-phonon collision frequency at electron temperatures on the order of $0.05T_F$ for copper, where T_F is the Fermi temperature (7 eV for Cu).^{18,19} Thus, the contribution of the electron-electron collisions to laser light absorption is important even at low temperature. This contribution is usually dominant in the temperature domain up to T_F . As the temperature increases further ($T_e > T_F$) a metal-plasma transition occurs, and the absorption is defined by the Coulomb electron-ion-collision frequency, which decreases with electron temperature as $T_e^{-3/2}$. Correspondingly, absorption starts to decrease with increasing electron temperature, in agreement with the experimental data.^{11,14} Note that, in a plasma phase, the electron-electron collisions may contribute somewhat to laser light absorption for low- Z plasma.²⁰

One more effect, which can be expected to change the absorption coefficient, is the nonthermal disordering of lattice state (nonthermal melting). In Cu such disorder occurs at an electron temperature ~ 3 eV that is an order of magnitude higher than the typical electron temperature at which the e - e collision contribution already starts to dominate over the e -phonon collisions. On the other hand, the experimental evidence for significant effect of nonthermal melting on the noble-metal reflectivity of femtosecond laser pulse remains inconclusive so far.²¹ In addition, there is uncertainty about typical time scales estimated for nonthermal melting to occur, ranging from ~ 100 fs (Ref. 21) to ~ 1 ps (Ref. 2). Thus, we do not believe that nonthermal melting contributes to the reflectivity increase at low intensity ($I \sim 1 \times 10^{12} - 3 \times 10^{12}$ W cm⁻²) because the electron temperature is quite low ($\sim 0.5 - 1$ eV) and laser pulse probably ends before nonthermal melting happens. Above this range, there is a lack of any suitable model for such nonthermal disordering, and thus we restrict ourselves to a smooth interpolation of the conductivity between the normal solid-state regime and the plasma regime of absorption.

To describe laser absorption in a broad electron temperature range, we use a smooth interpolation for dielectric permittivity between the Drude formula for solid metal²² and the corresponding formula for a plasma model. The effects of degeneracy and nonideality of a dense low-temperature plasma is taken into account by using a Fermi-Dirac electron distribution²³ and modified Coulomb logarithm.²⁴ The description of a classical high-temperature plasma is based on the exact solution of the electron kinetic equation,²⁰ which transforms to the well-known Spitzer-type formula in the strongly collisional limit.

The outline of the paper is as follows. In Sec. II the description of the experiment and experimental results are given. In Sec. III we present the theoretical model of laser-pulse absorption and localized heating. The discussion is presented in Sec. IV which includes comparison of the theory

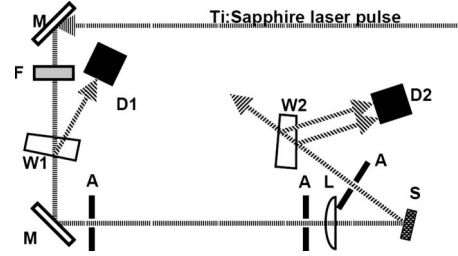


FIG. 1. Experimental setup for measuring the reflectivity of a laser-pulse incident on a flat reflective target. The labels in the diagram correspond to: M, aluminum mirrors; F, NG absorbing glass filters; A, apertures; W1, 2° fused silica wedge; W2, fused silica window; L, 15 cm focal length BK7 planoconvex lens; S, flat reflective sample on a 3D translation stage; D1 and D2, photodiodes.

and experimental data. The conclusions are given in Sec. V.

II. EXPERIMENTAL PROCEDURE AND RESULTS

Experimental measurements of the femtosecond reflectivity of copper were made using a commercial regeneratively amplified femtosecond Ti:sapphire laser system.²⁵ A pulse width of 150 fs FWHM was used for the experiments, measured using a commercial single-shot autocorrelator²⁶ with 20 fs resolution assuming a Gaussian pulse shape. The spatial profile of the output pulse was Gaussian down to approximately 10% intensity level with no hot spots as monitored with a Spiricon SP-980 camera at the focal spot of a 1 m lens. A 100 nm copper thin-film sample was used as a target, which was sputtered onto a silicon substrate with a 100 nm chromium thin-film binding layer between the copper layer and silicon substrate. The rms roughness of the surface was a few tenths of a nanometer as measured using a commercial white-light interferometer.²⁷ The copper thin-film sample was stored in a nitrogen environment to minimize oxidation of the surface before experimentation.

The experimental setup is shown in Fig. 1. The target was mounted on a commercial three-dimensional (3D) motorized translation stage and irradiated at approximately 7° angle of incidence with the incident laser s polarized. The pulse energy was controlled by a combination of a half-wave plate followed by a Glan polarizer at the output of the laser. Further energy attenuation was achieved using absorbing glass filters. The dispersion through these filters was negligible, adding at most a few femtoseconds to the pulse width, and was not considered in this work.

The pulse energy was measured at a kilohertz repetition rate by using a power meter with an accuracy of 1% (Spectra-Physics Model 407A) placed after the lens to calibrate the photodiode, D1 in Fig. 1. This calibrated photodiode was subsequently used for shot-to-shot energy measurements. The output of each photodiode was coupled into a 200 pF capacitor in parallel with a 1 M Ω resistor and was read out at 100 μ s after the laser pulse using a 50 MHz bandwidth digital oscilloscope. This time delay in measurement was employed to avoid interference from electrical noise from the laser firing at $t=0$. The precision of the pho-

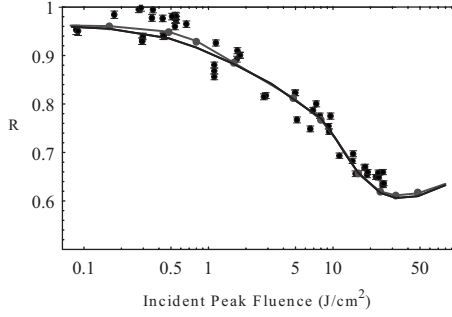


FIG. 2. Measured reflectivity of 800 nm 150 fs pulses from a copper surface as a function of peak incident energy fluence (in J/cm^2 , black points) in comparison with theoretical results (gray line with gray points). Black solid line corresponds to the model with zero heat flux.

todiode measurements was approximately 1%.

A fast photodiode at the output of the laser (not shown) monitored the femtosecond leakage pulse to determine the prepulse contrast ratio compared to the main pulse. The typical contrast ratio achieved was 3×10^4 . At these low levels, the prepulse was not expected to perturb the sample prior to the arrival of the main pulse.

The copper sample was placed at the focus of a 15 cm focal length lens to an accuracy of better than a millimeter, within the Rayleigh range of the focus. The calibration of 100% reflectivity for detector D2 was carried out using a high-reflectivity dielectric mirror at very low intensities. After calibration, the target was mounted and placed in the sample position, indicated by the reflected beam passing through the apertures. The incident-beam waist and laser fluence were measured by making single-shot ablation spots at different intensities, and measuring the ablation diameters with a white-light interferometer.²⁷ The details of the technique for calculating the beam diameter and resultant laser fluence are given in Ref. 8.

The repetition rate of the Ti:sapphire was reduced to single-shot mode and a clean fresh spot on the sample was irradiated with every shot. Measurements started at incident fluences a couple of orders of magnitude below the ablation threshold to verify the small-signal reflectivity of the target. Reflectivity was measured in random triplicates to avoid systematic errors by selecting incident pulse energies over the intensity range described earlier and making repeat measurements to observe the variability in the reflectivity for each intensity. Several samples had been used over several experiments with the resultant measured reflectivities plotted in Fig. 2. One can see that above an incident fluence of $1 \text{ J}/\text{cm}^2$ the absorption increases significantly with fluence.

III. DESCRIPTION OF THE MODEL

The description of target heating and ablation in short laser-pulse interaction with solid target is usually based on a two-temperature model.^{5,15,17} Here we are interested in femtosecond laser-pulse absorption and localized heating (near the target-vacuum interface) only, i.e., we consider only the first stage of laser-plasma interaction. In this case, it is suf-

ficient to assume a model of a semibounded medium, and consider only equations for the electron temperature, T_e , and the laser field, E , assuming ions to be cold and immobile. The equation for electron temperature is given by

$$C_e \frac{\partial T_e}{\partial t} - \frac{\partial}{\partial x} \left(\kappa [T_e(x)] \frac{\partial T_e}{\partial x} \right) = Q_L(x), \quad (1)$$

where C_e is the electron specific heat and κ is the electron heat conductivity. The heat deposition rate due to laser radiation, Q_L , is defined in the standard way by

$$Q_L(x) = \omega \text{Im}[\epsilon(t,x;\omega)] \frac{|E(t,x)|^2}{8\pi}, \quad (2)$$

where $\epsilon(t,x;\omega)$ is the target dielectric permittivity at the laser radiation frequency ω . Here we use the local approximation for Q_L , with the assumption of negligible effect of spatial dispersion that is justified both for solids and for plasmas with electron temperature up to several hundred electron volts.

To derive the electric field inside the target, $E(t,x)$, we solve a wave equation for the plane monochromatic wave incident from $x=-\infty$ onto a plane target surface located at $x=0$:

$$\frac{\partial^2 E(t,x)}{\partial x^2} + \frac{\omega^2}{c^2} \epsilon(t,x;\omega) E(t,x) = 0, \quad (3)$$

with boundary conditions $E(t,x \rightarrow \infty) = 0$ and $-i(c/\omega) \partial_x E(t,x)|_{x=0} + E(t,x)|_{x=0} = 2E_0(t)$, where $E_0(t)$ is the amplitude of the incident electromagnetic wave. For the incident electromagnetic field a Gaussian laser-pulse intensity, I , profile is assumed, $I(t) = (cE_0^2/8\pi) \exp[-(2 \ln 2)^2 (t - 2\tau)^2 / \tau^2]$, where τ is the laser-pulse duration defined as the FWHM. The absorption (A) and reflection (R) coefficients averaged over space (x) and time (t) are defined as follows:

$$\langle A \rangle = \frac{\int_0^{4\tau} dt \int_0^\infty dx Q_L(t,x)}{\int_0^{4\tau} dt I(t)}, \quad \langle R \rangle = 1 - \langle A \rangle. \quad (4)$$

The solution of the set of Eqs. (1) and (3) describes target heating, laser light absorption, reflection, penetration, and electron temperature profile inside the target.

To solve Eqs. (1) and (3) the target characteristics C_e , κ , and ϵ should be specified as functions of electron temperature. For a classical hot plasma the electron specific heat is independent of temperature, $C_e^p = 3/2 n_e$. For a metal at $T_e < T_F$, assuming that electrons are partially degenerated, the electron specific heat is proportional to electron temperature $C_e^m = \pi^2 T_e n_e / 2 T_F$. The simplest model for C_e is a smooth interpolation between these two limits^{15,17} as given by

$$C_e = n_e \frac{3\pi^2 T_e}{\sqrt{36T_F^2 + 4\pi^4 T_e^2}}. \quad (5)$$

To describe the electron density n_e , which is a key parameter of the theory, one has to properly evaluate an effective ion charge, $Z(n_e = Z n_i)$, where n_i is the atom density. For copper

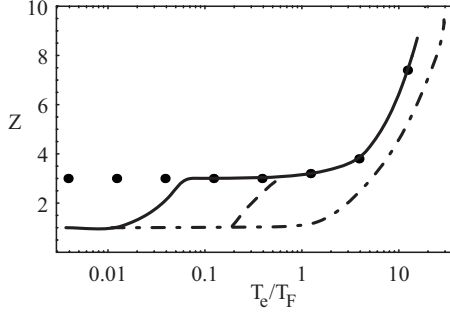


FIG. 3. Our $Z(T_e)$ dependence for Cu (solid line) in comparison with that from Refs. 29 (dashed line), 30 (points), and 32 (dashed-dotted line).

at the room temperature we take $Z = +1$, corresponding to excitation of s -shell electrons. A temperature increase results in thermal excitation of the low d -band electrons, which change the electron property of Cu.²⁸ To account for this change we assume an increase in effective average ion charge Z up to $Z = +3$ in the temperature range from $0.01T_F$ to $0.06T_F$ and saturation at higher temperatures up to T_F . This assumption allows one to adjust the temperature dependence of specific heat in Eq. (5) to the result of the numerical calculation of Ref. 28. Note that quasistationary value $Z = +3$ also has been predicted in Refs. 29 and 30. The fit for Z used for calculating laser absorption is presented in Fig. 3. The specific heat in Eq. (5) calculated with the proposed fit for effective ion charge Z is in a good agreement with the results in Ref. 28, where a specific heat for copper was calculated by using an exact electron density of state model as shown in Fig. 4.

The plasma dielectric permittivity can be calculated following the approach of Refs. 20 and 23 (cf. Ref. 24)

$$\epsilon = 1 - i \frac{\omega_{pe}^2}{T_F^{3/2}} \int_0^\infty d\varepsilon \frac{g\varepsilon^{3/2}}{2\omega\nu_{11}} \frac{\partial f_e}{\partial \varepsilon}, \quad T_F = (3\pi^2 n_e)^{2/3} \frac{\hbar^2}{2m_e}, \quad (6)$$

where f_e is the electron distribution function, which is a function of the electron energy ε , $g=2$ is the electron-spin degeneracy, $\omega_{pe} = \sqrt{4\pi e^2 n_e / m_e}$ is the electron plasma frequency, \hbar is the reduced Planck constant, and e and m_e are the electron charge and mass. We also introduced a renormalized collision frequency ν_{11} in such a way as to recover the permittivity of an ideal plasma²⁰ for temperature $T_e \gg T_F$. In

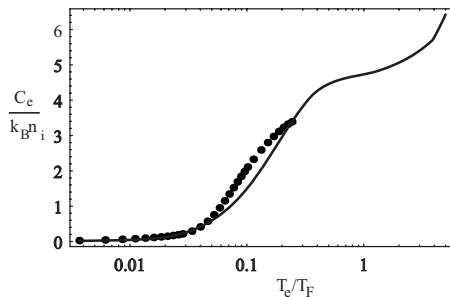


FIG. 4. Electron specific heat [Eq. (5)] (solid line) in comparison with that from Ref. 28 (points)

the local approximation the plasma expression for the renormalized frequency (as we only consider) results in $\nu_{11} = -i\omega + \sqrt{9\pi/2}(T_e/2\varepsilon)^{3/2} \nu_{ei}^T G(\omega, Z)$. The function $G = [\nu_{ei}^T / \gamma_\sigma + (1-2i)\omega] / [\nu_{ei}^T + (1-2i)\omega]$ accounts for the electron-electron collision effect in a plasma, where $\gamma_\sigma = (0.87 + Z)/(2.2 + Z)$ and $\nu_{ei}^T = 4\sqrt{2\pi} Z n_e e^4 \Lambda / 3m_e^{1/2} T_e^{3/2}$ is the electron-ion-collision frequency. The effects of a nonideal plasma are accounted for by the Coulomb logarithm, Λ (Ref. 24):

$$\Lambda = \frac{1}{4} \log \left[1 + \left(\frac{r_D + r_0 + l + \lambda}{l + \lambda_B/2} \right)^{1/4} \right], \quad (7)$$

where $1/r_D^2 = 4\pi e^2 n_e / \sqrt{T_e^2 + T_F^2}$ is the electron Debye radius with the degeneracy correction, $\lambda_B = \hbar / m_e v$ is the DeBroglie wavelength, $l = Ze^2 / m_e v^2$ is the classical distance of closest approach, and $v = \sqrt{2\varepsilon / m_e}$. Following Ref. 23 we use the minimal value for Coulomb logarithm $\Lambda_{\min} = 2$, i.e., $\Lambda = \max(\Lambda, \Lambda_{\min})$.

The distribution function of electrons can be presented in the form of a Fermi-Dirac function $f_e = 1 / (1 + \exp[(\varepsilon - \mu) / T_e])$, where a chemical potential μ is defined from the relation:

$$n_e = \frac{m_e^{3/2}}{\pi^2 \hbar^3 \sqrt{2}} \int_0^\infty d\varepsilon g \sqrt{\varepsilon} f_e. \quad (8)$$

In the limit of high temperature $T_e \gg T_F$, the chemical potential has the form $\mu = T_e \ln[8(T_F/T_e)^{3/2} / (3g\sqrt{\pi})]$. In this limit, the Fermi-Dirac distribution transforms to the Maxwellian distribution and for dielectric permittivity [Eq. (6)] we recover the result of Ref. 20:

$$\epsilon_p = 1 + i \frac{\omega_{pe}^2}{T_e^{5/2}} \sqrt{\frac{2}{\pi}} \int_0^\infty d\varepsilon \frac{\varepsilon^{3/2} \exp(-\varepsilon/T_e)}{3\omega\nu_{11}}. \quad (9)$$

Equation (6) is well suited for calculation of the dielectric permittivity at $T_e > T_F$ because the renormalized collision frequency described above is based on Coulomb collisions and is applicable only for a plasma. For solid state, in the limit of low electron temperatures $T_e < T_F$, one cannot use the Coulomb collision frequency as an effective collision frequency. The metal dielectric permittivity is described by the Drude formula

$$\epsilon_m = 1 - \frac{\omega_{pe}^2}{\omega(\omega + i\nu_{\text{eff}})}. \quad (10)$$

Note that when a collision frequency does not depend on electron energy, one can derive Drude formula (10) from Eq. (6) with $\nu_{11} = -i\omega + \nu_{\text{eff}}$. Following the model in Ref. 15 we use an expression for the effective collision frequency as $\nu_{\text{eff}} = \min[\nu_{e\text{-ph}} + \nu_{e\text{-e}}, \nu_c]$. Here $\nu_{e\text{-ph}} = k_s e^2 T_i / \hbar^2 v_F$ is the electron-phonon collision frequency, $v_F = \sqrt{2T_F/m_e}$ is the Fermi velocity, T_i is the ion temperature, $\nu_{e\text{-e}} = A_T T_e^2 / \hbar T_F$ is the electron-electron collision frequency, and $\nu_c = \sqrt{v_F^2 + T_e/m_e} / r_0$ is the maximum possible collision frequency, following from the condition that the electron mean-free path cannot be smaller than the ion sphere radius $r_0 = (3/4\pi n_i)^{1/3}$. We use the room temperature for T_i . Two fit-

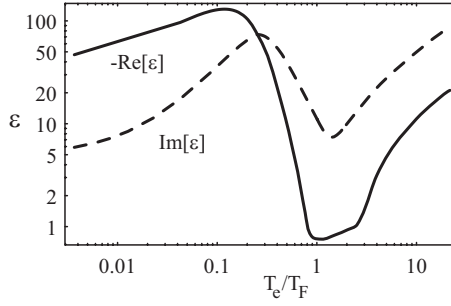


FIG. 5. Real (solid line) and imaginary (dashed line) parts of the dielectric permittivity of copper for $\omega=2.355 \times 10^{15} \text{ s}^{-1}$ and $n_i=8.47 \times 10^{22} \text{ cm}^{-3}$.

ting coefficients are introduced here for the effective collision frequency. The first one, as a scale factor for the electron-phonon collision frequency, $k_s=5.3$ is chosen to fit absorption for room temperature and the second one, A_T , is a parameter which adjusts for the quantitative uncertainty in a contribution of the electron-electron collisions. In our model, we use $A_T=3$ for a copper target, which provides the best agreement with experimental data on laser light reflectivity.

For $T_e > 3T_F$ we use the plasma expression for the electron dielectric permittivity, and for $T_e < 1/3T_F$ we use the Drude model for it. In the intermediate domain $1/3T_F < T_e < 3T_F$ we use the following interpolation¹⁵

$$\epsilon = -(\text{Re}[\epsilon_m]^4 + \text{Re}[\epsilon_p]^4)^{0.25} + i(\text{Im}[\epsilon_m]^4 + \text{Im}[\epsilon_p]^4)^{0.25}. \quad (11)$$

The electron temperature dependence of this dielectric permittivity for copper is shown in Fig. 5.

We approximate the electron heat conductivity in the entire range of the electron temperature by the expression $\kappa = \sqrt{\kappa_p^2 + \kappa_m^2}$, where $\kappa_p = 128(0.24 + Z)n_e T_e / [3\pi(4.2 + Z)m_e v_{ei}^T]$ is the plasma Spitzer heat conductivity and $\kappa_m = C_e^m v_F^2 / 3v_{\text{eff}}$ is the heat conductivity of a metal. Here v_{eff} is the same effective collision frequency as in the electron dielectric permittivity.

Equation (1) was solved numerically with boundary conditions corresponding to zero heat flux at the vacuum-target interface, $\partial T_e / \partial x|_{x=0} = 0$, and constant temperature (room temperature) deep in the target ($x \rightarrow \infty$). To find the electric field inside the target, Eq. (3) was solved at each time step by using the inhomogeneous dielectric permittivity calculated with the current electron temperature profile.

IV. DISCUSSION

The dependence of the time-averaged target reflectivity given by Eq. (4) is plotted with the experimental data in Fig. 2 where it is seen that there is good agreement between the model and the experimental data. For low laser intensities, the reflection corresponds to 0.95 that coincides with small-signal reflectivity of a clean copper surface at room temperature. For laser intensities $I \geq 5 \times 10^{12} \text{ W cm}^{-2}$, the growth of electron temperature results in an increase in laser light absorption (and decrease in reflectivity). The increasing effective collision frequency due to electron-electron collisions

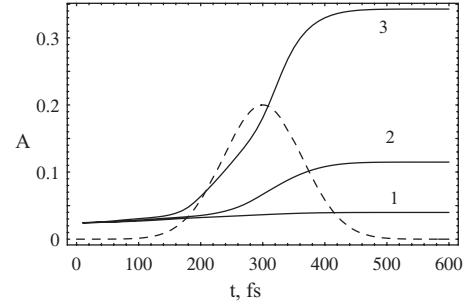


FIG. 6. Time evolution of the absorption coefficient of Cu foil irradiated by a laser pulse of 150 fs duration with maximum intensity of (1) 10^{12} , (2) 10^{13} , and (3) 10^{14} W/cm^2 . The dashed curve shows the Gaussian laser-pulse profile.

(with corresponding contribution $\propto T_e^2$) and increasing effective degree of ionization Z are responsible for the absorption increase. The absorption reaches a maximum for an intensity of the order of $I \sim 2 \times 10^{14} \text{ W cm}^{-2}$ and slowly decreases with further increase in laser fluence. The latter is relevant to the laser-plasma interaction regime. On the whole, the behavior of copper reflectivity qualitatively agrees with that of aluminum reflectivity.¹⁴

The time evolution of the absorption coefficient for a Cu foil given in Fig. 6 clearly shows that absorption ends 100 fs after the maximum of laser pulse reaches the target surface. This justifies our assumption that processes with time scales longer than a few hundred femtoseconds have negligible effect on absorption. The dependence of maximum surface temperature of copper foil on laser-pulse intensity is shown in Fig. 7. It demonstrates that for 150 fs laser pulse an electron-ion plasma appears at laser intensities higher than $10^{13} \text{ W cm}^{-2}$ once the electron temperature exceeds 3 eV.

The spatial profiles of the absorbed power, Q_L given in Eq. (2), for different laser intensities are shown in Fig. 8. The absorbed power is proportional to the laser intensity inside the target and the electrical conductivity of the target. Because the laser electric field decreases monotonically inside the target and the electrical conductivity is sensitive to the electron temperature profile, having a maximum at a temperature of the order of the Fermi temperature, the absorbed power profile may have a nontrivial shape. For low intensities when the target is not heated above the Fermi temperature the electrical conductivity decreases with x inside the target and the absorbed power follows the exponential profile of the laser intensity inside the surface. With increasing intensity, when the target can be heated above the Fermi tem-

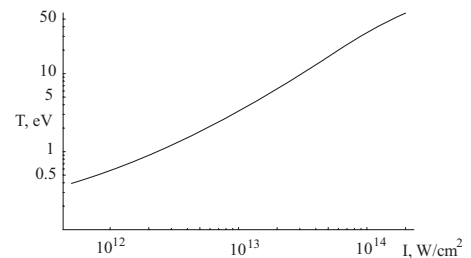


FIG. 7. The maximum of the electron surface temperature of Cu foil as a function of peak incident laser intensity.

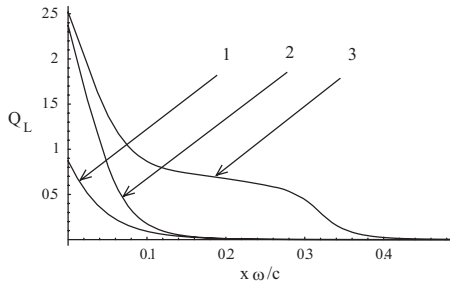


FIG. 8. The spatial profile of the absorbed power Eq. (2), for laser intensities (1) 10^{12} , (2) 10^{13} , and (3) 10^{14} W cm^{-2} at the instant when the peak of the laser pulse reaches the target surface ($t = 300$ fs).

perature, the absorbed power profile plateaus inside the target due to the nonmonotonic behavior of conductivity versus electron temperature. For example, at an intensity of 10^{14} W cm^{-2} the laser-plasma interaction results in the absorbed power profile with a well pronounced plateau inside the target as seen in Fig. 8.

The electron temperature profile at the end of simulation (at 600 fs) and the evolution of surface temperature for a copper target irradiated by a laser pulse with intensity 10^{14} W cm^{-2} are presented in Figs. 9 and 10, respectively. To reveal the effect of electron heat transport, the calculations with zero heat flux are also presented. The electron heat flux from the skin layer results in a decrease in the surface temperature due to energy transport by a heat wave propagated into the target. The effect of heat flux is important for a plasma with relatively high electron temperature $T_e \gtrsim 20$ eV.

Our study shows that accounting for the electron heat transport does not significantly affect integrated laser light reflectivity for the intensities $\leq 10^{14}$ W/cm^2 and the present pulse duration of interest ~ 150 fs. However, electron heat transport is important for correct determination of the electron temperature value and spatial temperature profile. Electron heat flux comes into play after electrons heat up to temperatures on the order of 10–20 eV, which happens only after the peak of the laser pulse reaches the target (see Fig. 10). By this instant in time, the main part of the laser light is already absorbed by the target. Moreover, for the electron temperature range $20 \text{ eV} < T_e < 100 \text{ eV}$, where the plasma is not too hot, the absorption coefficient varies weakly with tempera-

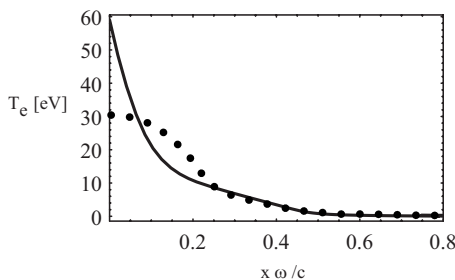


FIG. 9. The electron temperature profile for Cu foil irradiated by a laser pulse of 150 fs duration with maximum intensity of 10^{14} W cm^{-2} at the end of calculation ($t=600$ fs) with (dots) and without (solid line) accounting for the electron heat transport.

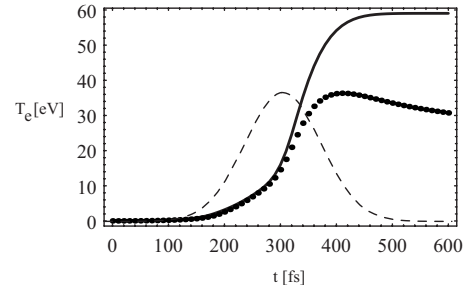


FIG. 10. Time evolution of the electron surface temperature of Cu foil irradiated by laser pulse of 150 fs duration with maximum intensity of 10^{14} W cm^{-2} with (dots) and without (solid line) accounting for the electron heat transport. The dashed curve shows the Gaussian laser-pulse profile.

ture. Correspondingly, the temperature redistribution within the skin layer due to heat transport does not noticeably change the contribution to the integrated absorption from the decaying part of the laser pulse. Thus, the average value of laser light reflectivity for both temperature profiles, with and without accounting for the heat flux, is approximately the same.

In the presented absorption model, the lattice heating due to electron-lattice energy exchange is neglected and ions are assumed to be cold (at room temperature). Fast heating of the lattice could result in a considerable increase in the contribution of the electron-lattice collision frequency to the effective collision frequency and change the laser absorption. One may estimate the lattice temperature as $T_i \sim T_e t / t_r$, where t_r is the characteristic electron-ion relaxation time. In accordance with Ref. 13, $t_r \sim (30-40)$ ps. Thus, at the end of laser pulse (about 300 fs), the ion temperature reaches about 1% of the electron temperature, which is about 3000 K for a laser intensity of 10^{14} W cm^{-2} . On the other hand, in Ref. 28 it was noted that relaxation rate t_r itself depends on the electron temperature that could result in smaller value of t_r as compared to that estimated in Ref. 13. On this basis one may estimate that at the end of laser pulse the ion temperature could be about 9000 K. While it is considerably higher than room temperature, nevertheless, lattice heating can be ignored because its relative contribution to the effective collision frequency decreases with electron heating since the electron-electron collision contribution becomes strongly dominant.

The electromagnetic field penetrates inside the target to a skin depth of 20–60 nm,^{31,32} which is typical for solid density metal plasmas. The characteristic electron temperature scale length is also comparable to the skin depth where the plasma formed is strongly inhomogeneous during the laser-pulse interaction. Therefore the commonly used model of homogeneous temperature is not applicable for the description of absorption (see also Refs. 15 and 17). It significantly overestimates laser absorption and could not provide agreement with experimental data.

V. CONCLUSION

Experimental measurements of absorption of 150 fs laser pulses have been made from clean copper surfaces at a wave-

length of 800 nm for intensities in the range of 6×10^{11} – 1.6×10^{14} W cm⁻². This is an important regime for many applications of femtosecond pulses and for the creation of preplasmas in many femtosecond relativistic laser-plasma experiments. We have found that the absorption increases rapidly at approximately 3×10^{12} W cm⁻² and reaches a value approaching 40% at intensities above 10^{14} W cm⁻². A theoretical model has been developed taking into account the transition from an electron-phonon dominated cold collision regime to an electron Coulomb dominated plasma collision regime. It allows the derivation of instantaneous and integrated coefficients of absorption, the spatiotemporal absorbed power profile, and the spatiotemporal electron temperature distribution.

Taking into account the Gaussian temporal and spatial profiles of the experimental laser pulse, numerical integration of the theoretical model gives very good agreement with

the experimental measurements. An increase in absorption to an intensity of 2×10^{14} W cm⁻² is observed after which the heated surface starts to behave as a hot plasma exhibiting decreasing absorption with intensity. The obtained characteristics of a surface plasma on subpicosecond time scale clears the way for ablation studies at a quantitative level.

ACKNOWLEDGMENTS

The authors thank N. G. Karlykhanov, V. A. Lykov, W. Rozmus, and A. T. Sapozhnikov for fruitful discussions. This work was supported in part by the Russian Foundation for Basic Research, the International Science and Technology Center (Project No. 2289), the Natural Sciences and Engineering Research Council of Canada, and the Canadian Institute for Photonic Innovations.

-
- ¹S. D. Brorson, J. G. Fujimoto, and E. P. Ippen, *Phys. Rev. Lett.* **59**, 1962 (1987).
- ²C. Guo and A. J. Taylor, *Phys. Rev. B* **62**, 5382 (2000).
- ³J. Hohlfeld, S.-S. Wellershoff, J. Güdde, U. Conrad, V. Jähnke, and E. Matthias, *Chem. Phys.* **251**, 237 (2000).
- ⁴D. von der Linde, K. Sokolowski-Tinten, and J. Bialkowski, *Appl. Surf. Sci.* **109-110**, 1 (1997).
- ⁵S. I. Anisimov, B. L. Kapeliovich, and T. L. Perelman, *Sov. Phys. JETP* **39**, 375 (1974).
- ⁶S. I. Anisimov and B. Rethfeld, *Proc. SPIE* **3093**, 192 (1997).
- ⁷C. Momma, S. Nolte, B. N. Chichkov, F. von Alvensleben, and A. Tünnermann, *Appl. Surf. Sci.* **109-110**, 15 (1997).
- ⁸S. E. Kirkwood, A. C. Van Popta, Y. Y. Tsui, and R. Fedosejevs, *Appl. Phys. A: Mater. Sci. Process.* **81**, 729 (2004).
- ⁹S. E. Kirkwood, M. T. Taschuk, Y. Y. Tsui, and R. Fedosejevs, *J. Phys.: Conf. Ser.* **59**, 591 (2007).
- ¹⁰I. V. Cravetchi, M. T. Taschuk, Y. Y. Tsui, and R. Fedosejevs, *Anal. Bioanal. Chem.* **385**, 287 (2006).
- ¹¹D. F. Price, R. M. More, R. S. Walling, G. Guethlein, R. L. Shepherd, R. E. Stewart, and W. E. White, *Phys. Rev. Lett.* **75**, 252 (1995).
- ¹²R. Fedosejevs, R. Ottmann, R. Sigel, G. Kuhnle, S. Szatmari, and F. P. Schafer, *Phys. Rev. Lett.* **64**, 1250 (1990); *Appl. Phys. B: Photophys. Laser Chem.* **50**, 79 (1990).
- ¹³K. Eidmann, J. Meyer-ter-Vehn, T. Schlegel, and S. Huller, *Phys. Rev. E* **62**, 1202 (2000).
- ¹⁴H. M. Milchberg, R. R. Freeman, S. C. Davey, and R. M. More, *Phys. Rev. Lett.* **61**, 2364 (1988).
- ¹⁵M. B. Agranat, N. E. Andreev, S. I. Ashitkov, M. E. Veisman, P. R. Levashov, A. V. Ovchinnikov, D. S. Sitnikov, V. E. Fortov, and K. V. Khishchenko, *JETP Lett.* **85**, 271 (2007).
- ¹⁶A. A. Abrikosov, *Fundamentals of the Theory of Metals* (North-Holland, Amsterdam, 1988); N. W. Ashcroft and N. D. Mermin, *Solid State Physics Holt* (Reinhard and Winston, New York, 1976).
- ¹⁷D. Fisher, M. Fraenkel, Z. Henis, E. Moshe, and S. Eliezer, *Phys. Rev. E* **65**, 016409 (2001).
- ¹⁸A. P. Kanavin, I. V. Smetanin, V. A. Isakov, Y. V. Afanasiev, B. N. Chichkov, B. Wellegehausen, S. Nolte, C. Momma, and A. Tünnermann, *Phys. Rev. B* **57**, 14698 (1998).
- ¹⁹B. Chimier, V. T. Tikhonchuk, and L. Hallo, *Phys. Rev. B* **75**, 195124 (2007).
- ²⁰A. V. Brantov, V. Yu. Bychenkov, and W. Rozmus, *JETP* **106**, 983 (2008).
- ²¹D. V. Fisher, Z. Henis, S. Eliezer, and J. Meyer-Ter-Venn, *Laser Part. Beams* **24**, 81-94 (2006).
- ²²N. W. Ashcroft and N. D. Mermin, *Solid State Physics* (Holt, Rinehart, and Winston, New York, 1976), translated in Russian (Mir, Moscow, 1979), Vol. 1.
- ²³Y. T. Lee and R. M. More, *Phys. Fluids* **27**, 1273 (1984).
- ²⁴A. Ya. Polishchuk, *Teplofiz. Vys. Temp.* **28**, 877 (1990).
- ²⁵Spectra-Physics, Inc., 1335 Terra Bella Ave., Mountain View, CA 94039, USA.
- ²⁶Positive Light, Inc., 101 Cooper Ct., Los Gatos, CA 95032, USA.
- ²⁷Zygo Corporation, Laurel Brook Rd., Middlefield, CT 06455-0448, USA.
- ²⁸Z. Lin, L. V. Zhigilei, and V. Celli, *Phys. Rev. B* **77**, 075133 (2008).
- ²⁹G. E. Rolader and J. H. Batteh, *IEEE Trans. Plasma Sci.* **17**, 439 (1989).
- ³⁰W. Ebeling, A. Forster, V. Fortov, V. Gryaznov, and A. Polishchuk, *Thermophysical Properties of Hot Dense Plasmas* (Teubner, Stuttgart, Leipzig, 1991).
- ³¹Max Born and Emil Wolf, *Principles of Optics*, 7th ed. (Cambridge University Press, Cambridge, 1999), Chap. 14.
- ³²*CRC Handbook of Chemistry and Physics*, 84th ed., edited by David R. Lide (CRC, Boca Raton, Florida, 2003).